Oxygen diffusion and oxide phase formation in iron under swift heavy ion irradiation

Tobias Roller and Wolfgang Bolse*
Institut für Strahlenphysik, Universität Stuttgart, Allmandring 3, 70569 Stuttgart, Germany
(Received 8 August 2006; revised manuscript received 16 November 2006; published 9 February 2007)

While irradiating thin iron films deposited on silicon wafers with swift heavy ions in the energy range of a few MeV/amu, we have observed that the iron surface oxidizes due to the residual oxygen in the irradiation chamber, induced by the energy deposition by the ion. We have investigated these processes in detail using Rutherford backscattering spectrometry and conversion electron Mössbauer spectroscopy. We found that two different types of oxidation processes were active, depending on the electronic energy loss of the incident ions. Irradiations above the track formation threshold S_{ec}^{Fe} of iron resulted in diffusion-controlled dissolution of oxygen in the iron bulk. Below S_{ec}^{Fe}, but above the track formation threshold of iron oxide, chemical reaction and homogeneous oxide phase formation took place in a surface layer, while almost no oxygen diffusion into the iron bulk could be observed anymore. These phenomena are discussed in terms of the oxygen mobility in the excited ion tracks in iron and iron oxide. The effective diffusion constant estimated for swift heavy ion induced oxygen diffusion in iron is larger by a factor of 100–1000 than the one reported for thermally activated oxygen diffusion in molten iron.

DOI: 10.1103/PhysRevB.75.054107 PACS number(s): 61.80.Jh, 61.82.Bg, 66.30.−h

I. INTRODUCTION

The interest in materials modification using swift heavy ions (SHI) with energies of a few MeV/amu (i.e., at the maximum of the electronic stopping cross section) has significantly increased during the past 10 years, since it turned out that SHI may be a valuable tool for micro- and nanostructuring of surface layers and thin films.[1,2] The uniqueness of SHI results from the fact that the impact of a single ion drives the solid into a highly excited state, which is confined in a cylindrical volume of a few nm in diameter and some μm in length and surrounded by an unexcited "cold" lattice. The initial energy density deposited into the electronic system of the solid exceeds several eV/atom on the average, and is in part transferred into the lattice by Coulomb explosion or, more likely, by electron-phonon coupling, within some 10^{-14} s.[3,4] The average energy per atom near the ion path may significantly exceed the solid binding energies, and as a first-order approximation, the excited nanoscale region can be regarded as a melt, which because of its different density as compared to the solid is not only at high temperature but also at high pressure. Because of these extreme conditions and the very rapid cooling rates ($\approx 10^{14}$ K s), often a nonequilibrium structure is left on nanoscale lateral dimensions after the excitation has been dissipated into the bulk.

We have recently shown that, when the ion track passes through the interface of a layered system, significant atomic transport occurs from one layer to the other, provided that the track formation threshold in the electronic stopping power is exceeded by the given ion species in both materials, i.e., the deposited energy density is large enough to melt both materials along the ion's trajectory. We could show that this atomic transport occurs most likely by interdiffusion in the molten material.[5–7] In some cases not only does interface mixing occur upon SHI bombardment, but nonequilibrium phases are formed at the interface, as a consequence of the extreme conditions in the excited ion track and the rapid cooling down.[8]

In the present work we have investigated the incorporation of oxygen in iron during SHI irradiation at a temperature of 80 K and the subsequent irradiation-induced diffusion and oxide phase formation. It was already shown by Avasthi *et al.*[9] that SHI irradiation of iron in a standard accelerator vacuum results in surface oxidation. It was concluded that the oxygen stemmed from the residual oxygen partial pressure in the vacuum or from water adsorbed on the surface. The authors also estimated an effective diffusion coefficient, because of which they concluded that the oxygen diffusion in iron occurs in the molten ion track. In the present paper, we will show that oxygen not only diffuses into the iron, when the stopping power of the ion exceeds the track formation threshold of iron, but oxide phase formation occurs when it falls below. This happens because now the diffusivity is highly limited in iron while ion track formation is still possible in the oxide, resulting in a high mobility of oxygen in the oxide layer. Again, most likely because of the extreme conditions in the ion track, the oxide turns out to appear in a nonequilibrium high-temperature phase, which decays into the respective equilibrium phases upon thermal annealing.

II. EXPERIMENT

A. Sample preparation

Iron was deposited onto silicon wafers with or without a thermally grown silicon oxide layer, using reactive magnetron sputtering. By controlling the oxygen content in the argon working gas, one can determine the oxygen content of the deposited layer. In our case, pure iron layers as well as substoichiometric iron oxides FeO_x with $0 \leqslant x < 1$ were used with a homogeneous oxygen content over thicknesses of a few hundred nm. The Si wafers had a thickness of 250 μm.

B. Irradiation

The samples were irradiated at the Ionenstrahllabor of the Hahn-Meitner-Institut in Berlin. At this facility, heavy ions at

TABLE I. Electronic stopping power S_e for the ions used in this work [calculated with SRIM (Ref. 10)].

Ion	S_e [eV/(atoms × nm^{-2})]	
	in Fe	in Fe_2O_3
180 MeV $^{84}Kr^{12+}$	287	187
230 MeV $^{132}Xe^{15+}$	452	295
350 MeV $^{197}Au^{26+}$	604	395

energies of MeV/amu were available at sufficiently high beam currents so that the required ion fluences could be achieved within a few hours. The ions used in this work were $^{84}Kr^{12+}$ at 180 MeV, $^{132}Xe^{15+}$ at 230 MeV, and $^{197}Au^{26+}$ at 350 MeV. In this energy range, the electronic energy transfer S_e (see Table I) clearly dominates over the nuclear energy transfer S_n, which in all cases contributes to the total energy loss by less than 1%. It should be noted here that the S_e values given in Table I refer to the respective ions in the equilibrium charge states (Kr: 19–20, Xe: 22–23, Au: 26).[11] In all cases, these are larger than the initial charge states of the ions, which means that the electronic stopping power especially for Kr and Xe in the uppermost layer of a few nm thickness might be somewhat smaller.[12,13] The irradiations were carried out under normal ion incidence. The samples were fixed on a liquid nitrogen cooled Cu sample holder by means of silver paste. The temperature of the sample holder was monitored by a thermocouple and was found not to increase by more than 1 K next to the samples. The temperature difference between the sample surface and the sample holder during irradiation was estimated using the Fourier heat conduction equation,

$$j = -\lambda \frac{dT}{dz}. \quad (1)$$

As the heat flow, $j = \dot{\Phi} E_{\text{ion}}$, we took the total energy flux introduced by the ion. The typical ion flux was of the order of $\dot{\Phi} \approx 10^{10}$ cm^{-2} s^{-1} and the maximum ion energy $E_{\text{ion}} = 350$ MeV. Even if we assume a bad heat conductivity of $\lambda = 0.1$ W (mK)$^{-1}$ [for comparison, λ(Si) = 150 W (mK)$^{-1}$], the temperature increase at the surface stays below 15 K. Hence, beam heating can be excluded to contribute to the observed effects.

In order to keep a reference to the unirradiated state, only a part of the sample was irradiated, which ensures that during analysis the conditions are the same for the irradiated and the unirradiated samples.

C. Analysis

Rutherford backscattering spectrometry (RBS) was used to gain information about the chemical composition and depth profiles of the elements in the layers. These measurements were done at the DYNAMITRON accelerator of the Institut für Strahlenphysik at Universität Stuttgart. For the analysis of the samples, He^+ ions at 1 and 2 MeV were used at a scattering angle of 165°. The obtained spectra were evaluated employing the RUMP (Ref. 14) and NDF (Ref. 15) codes.

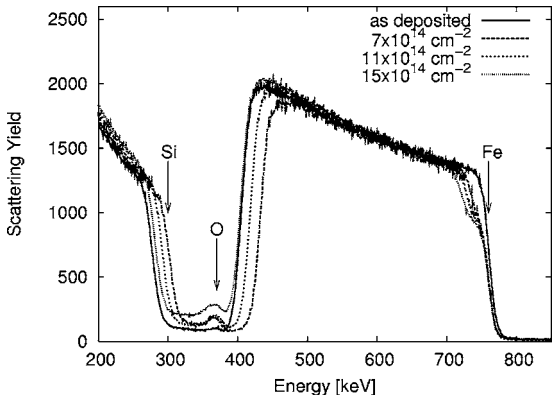

FIG. 1. RBS spectra before and after irradiation with 180 MeV $^{84}Kr^{12+}$ at several fluences

In addition to RBS, the samples were characterized using conversion electron Mößbauer spectrometry (CEMS). This method yields information about the phase of the iron and iron oxides and, furthermore, tells whether the sample is amorphous or crystalline. As the conversion electrons have a limited range in the sample, the measurement is only sensitive to the surface region. The maximum range is roughly 200 nm. For details of the technique, see Ref. 16.

III. RESULTS

A. Irradiation with 180 MeV Kr

After the irradiation of iron samples having little or no oxygen content with swift heavy ions, a clear incorporation of oxygen into the surface near regions can be detected, as was also reported in Ref. 9. For 180 MeV ^{84}Kr ions, RBS showed a plateaulike reduction of the iron yield at the surface, as can be seen in Figs. 1 and 2, indicating the formation of a new phase. In addition, oxygen could be detected in the RBS spectra of the irradiated samples. From the reduction of

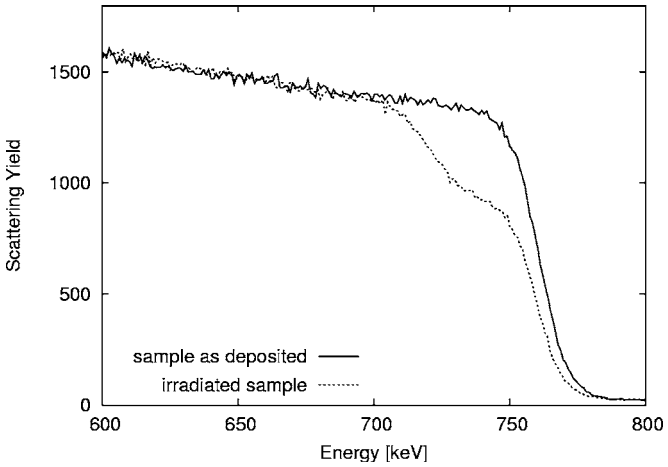

FIG. 2. RBS spectrum (iron edge) before and after irradiation with 180 MeV $^{84}Kr^{12+}$ at the highest fluence $\Phi = 15 \times 10^{14}$ cm^{-2}.

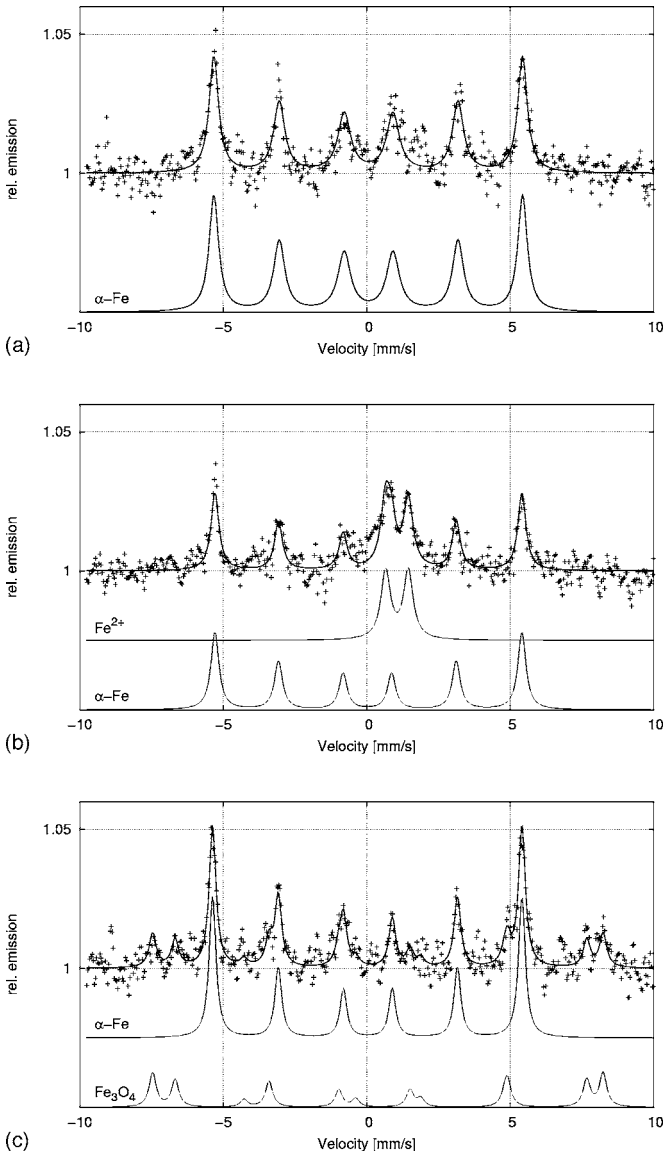

FIG. 3. Conversion electron Mössbauer spectroscopy (CEMS) of a sample consisting of 265 nm $FeO_{0.15}$ on silicon substrate. The experimental data were evaluated using the GOEMOSS code (Ref. 22). In addition to the fitted curve through the experimental data points, the components of the fit are displayed underneath each spectrum. Upper spectrum: unirradiated sample, shows only the α-iron sextuplet. Middle spectrum: after irradiation (15×10^{14} $^{84}Kr^{12+}/cm^2$ at 180 MeV). Apart from the α-iron sextuplet, a doublet can be seen, the isomer shift (1.05 mm/s) of which indicates the existence of Fe^{2+}. Lower spectrum: irradiated sample after annealing at 350 °C for 45 min. The Fe^{2+} doublet vanishes and the two sextets of the *A* and *B* site of magnetite appear.

the RBS yield at the iron edge, the composition of the new phase was calculated as $Fe_{0.91-1.0}O$.

In order to further characterize this phase, CEMS measurements have been performed (see Fig. 3). The spectrum of the sample before irradiation shows that most of the iron is in the α-Fe phase. The spectrum of the irradiated sample shows in addition a doublet centered at 1.05 mm/s. FeO normally has a cubic structure, where the Fe^{2+} exhibits an isomer shift of 1.055 mm/s, but, because of the lattice symmetry, no

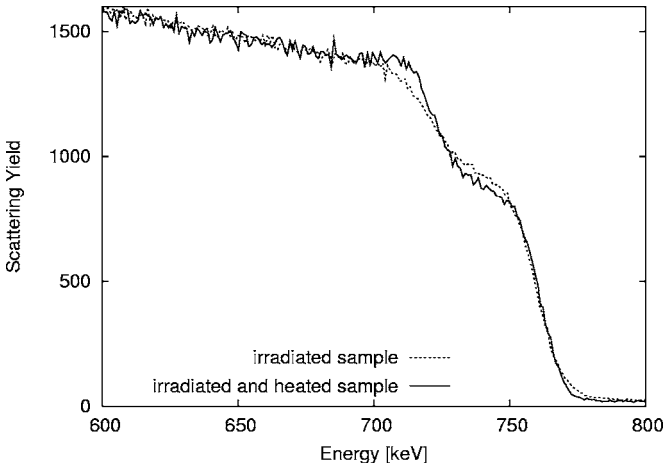

FIG. 4. RBS spectrum of the same sample as in Fig. 2, but after heating at 350 °C for 45 min.

quadrupole splitting.[17] However, as has been reported by Shirane *et al.*,[18] the Wüstite phase ($Fe_{0.92-0.95}O$), which is unstable at room temperature, exhibits an isomer shift of 1.15 mm/s and a quadrupole splitting of 0.32 mm/s, similar to what we have observed here. In addition, the composition of the new phase observed after ^{84}Kr-ion irradiation compares nicely with that of the Wüstite phase. Moreover, the iron-oxygen phase diagram[19] shows a transition from Wüstite ($Fe_{0.92-0.95}O$) to magnetite (Fe_3O_4) and α-Fe below $\approx$560 °C. Exactly this transition was observed after heating the sample in vacuum for 45 min at 350 °C. The respective CEMS spectrum shows indeed the appearance of the magnetite and the α-Fe phases (see Fig. 3, lower spectrum). This transition also shows up in the RBS spectrum in Fig. 4, where the rearrangement of oxygen and iron becomes visible as a slight change in the iron yield height in the surface near region and the increase of the steepness of the lower energy edge. We therefore conclude that the Kr irradiation resulted in the formation of a wüstite layer. The thickness of this layer, as determined from the RBS spectra, grows with the square root of the ion fluence (see Fig. 5) at a rate of $\frac{\sigma^2}{\Phi}=(80.1\pm2.4)$ nm^4, indicating a diffusion-controlled chemical

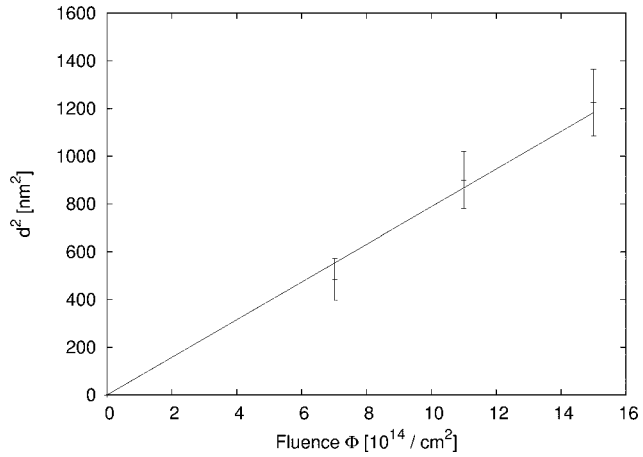

FIG. 5. The square of the thickness *d* of the wüstite layer as a function of the 180 MeV Kr-ion fluence Φ.

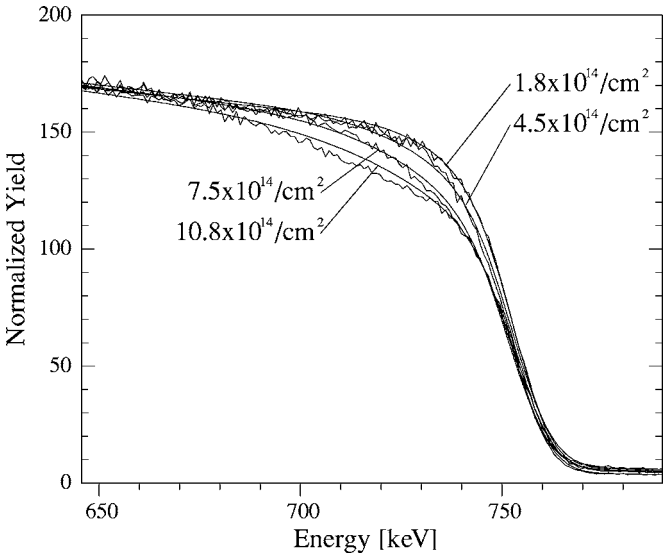

FIG. 6. RBS spectra of an iron surface layer for several irradiation fluences of 230 MeV $^{132}Xe^{15+}$. Also shown are simulations of a diffusion process considering an error-function oxygen profile (see text).

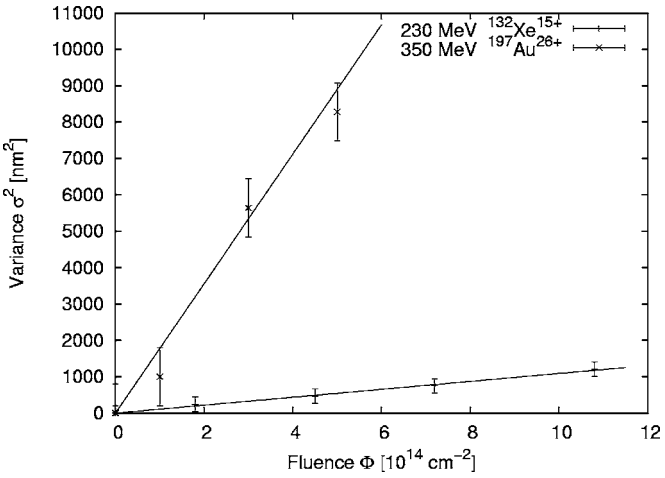

FIG. 7. Variance σ^2 of the oxygen diffusion profile in iron after irradiation with various fluences Φ of 230 MeV Xe and 350 MeV Au.

reaction.[20,21] In addition to the plateaulike region, an error-function-like diffusion profile into to the iron can be detected, the range of which, however, is smaller than the thickness of the oxide layer.

B. Irradiation with 230 MeV Xe and 350 MeV Au

In contrast to 180 MeV Kr irradiation, the irradiation of iron samples with Xe at 230 MeV or with Au at 350 MeV did not result in the formation of a homogeneous phase (which shows up as a plateau at the iron edge in the RBS spectra) but a continuously decreasing oxygen diffusion profile starting already at the surface. The iron edge of the RBS spectra for several irradiation fluences of 230 MeV Xe can be seen in Fig. 6. The spectra were fitted using an error-function-like oxygen profile,

$$C(x,\Phi) = C_0 \,\mathrm{erfc}\left(x\sqrt{\frac{\sigma^2(\Phi)}{2}}\right). \tag{2}$$

Here $C(x,\Phi)$ is the diffusant's concentration at depth x (surface: $x=0$) after irradiation with fluence Φ. C_0 is the oxygen concentration at the surface and σ^2 is the variance of the error function.

The plot of σ^2 versus the ion fluence Φ in Fig. 7 again reveals a linear relationship, with a proportionality constant $D' = \frac{\sigma^2}{\Phi}$. For the irradiation with 230 MeV Xe ions, we obtain

$$D' = (10.9 \pm 0.2) \times 10^{-27}\ \mathrm{cm}^4,$$

while for 350 MeV Au ions it becomes

$$D' = (17.8 \pm 3.0) \times 10^{-26}\ \mathrm{cm}^4.$$

IV. DISCUSSION

As we will discuss in the following, the difference in the oxidation behavior of iron during Kr irradiation and the irradiation with the heavier ions Xe and Au can be understood in terms of the formation of "molten" ion tracks above a threshold value S_{ec}, which differs for iron oxide and pure iron. Such track formation thresholds have been observed also before in other experiments. Dunlop and co-workers[23] reported a defect creation threshold for iron, which is at about $S_{ec}^{\mathrm{Fe}} = 400$ eV nm^2/at. The latter value is in good agreement with our calculations according to the thermal spike model by Toulemonde *et al.*[24] The results of these calculations for 230 MeV Xe and 350 MeV Au ions are shown in Fig. 8. According to this model, 230 MeV Xe ions ($S_e^{\mathrm{Fe}} = 452$ eV nm^2/at) are capable of driving the material only a little above its melting point within a radius of 3 nm at maximum for distinctly less than 1 ps. This means that the electronic energy loss of 230 MeV Xe in Fe is only slightly above the track formation threshold, which is in good agreement with the above-mentioned experimental threshold $S_{ec}^{\mathrm{Fe}} \approx 400$ eV nm^2/at. 350 MeV Au ions ($S_e^{\mathrm{Fe}} = 604$ eV nm^2/at), on the other hand, form a molten cylinder of more than 10 nm in diameter and drive the material significantly above its melting point for more than 1 ps. This allows for significant indiffusion of oxygen in the molten iron. 180 MeV Kr ions do not deposit sufficient energy to melt pure iron, which means that in this case no or only very little oxygen diffusion can take place in Fe.

For iron oxide, to our knowledge, no direct information about latent track formation and the respective thresholds is available. Unfortunately, because of the lack of knowledge of the parameters needed for the thermal spike calculations, also no theoretical prediction of the thresholds can be made. In our ion beam mixing experiments, however, we found that mixing of Fe_2O_3 and SiO_2 occurs as soon as the electronic stopping power exceeds a value of $S_{ec}^{Fe_2O_3} = (53 \pm 18)$ eV nm^2/at.[6] We are aware that mixing thresholds might not coincide with track formation thresholds, because hot electrons might be transferred to the less sensitive material across the interface with a more sensitive material and lead to mixing below the track formation threshold. This has been demonstrated by the experiments done by Leguay

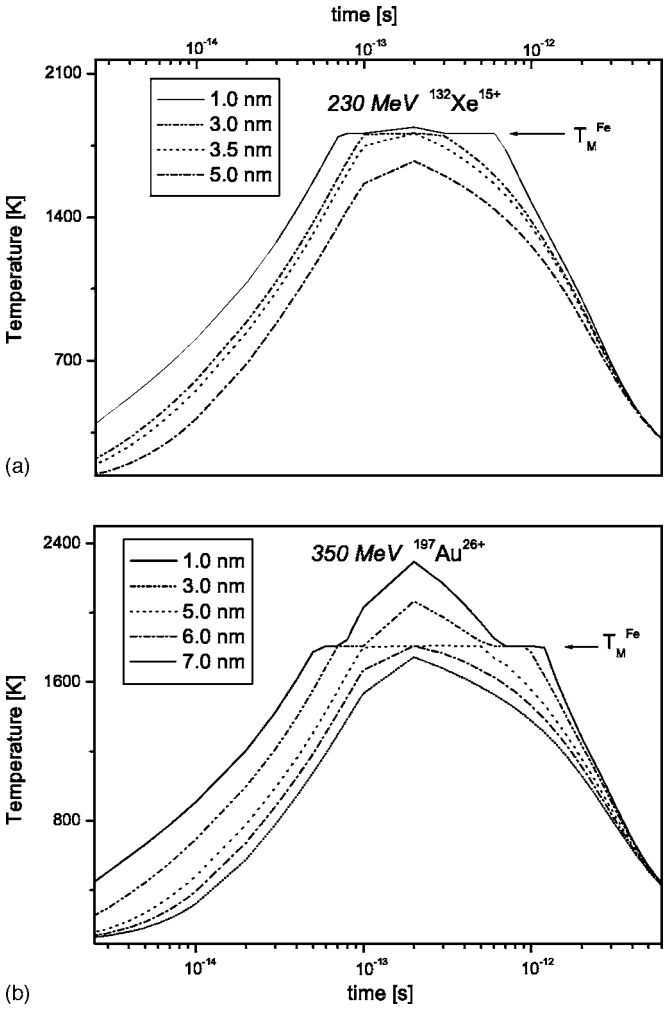

FIG. 8. Time dependence of the temperature at different radial distances from the track center for irradiations with 230 MeV Xe (upper diagram) and 350 MeV Au (lower diagram) according to calculations with the thermal spike model. The melting point of iron (1809 K) is indicated by the arrow.

et al.,[25] who showed that the otherwise completely S_e-insensitive Ni mixes with Ti when bombarding Ni/Ti interfaces with SHI. Chettah *et al.*[26] indeed predicted that also the Au (which is also insensitive in its bulk form) in thin Au/Fe multilayers may melt, if they were bombarded with SHI above the track formation threshold of iron. In fact, Rumbolz *et al.*[27] have observed that Au/Fe multilayers were smoothing under SHI irradiation at 80 K. Hence, mixing thresholds may be smaller than track formation thresholds. In the case of Fe_2O_3, we are, however, quite sure that both quantities do not differ very much, and the mixing threshold of $S_{ec}^{Fe_2O_3} = (53 \pm 18)$ eV nm^2/at, as a good approximation, can be regarded as the track formation threshold. We have investigated a series of oxide and nitride bilayers and found that the mixing thresholds in these materials agreed nicely with the theoretical track formation thresholds of the less sensitive material predicted by the semiempirical Szenes model.[6,28] Fe_2O_3 fully fits into this systematics.

In contrast to iron, in iron oxide the energy loss by 180 MeV Kr ions is above the track formation threshold and, hence, if a thin oxide layer is present on top of the iron surface (which will always be the case after handling the sample in air[29]), a 180 MeV Kr ion will generate a molten track inside this layer, which allows the oxygen to diffuse from the surface to the oxide-iron interface and to extend the oxide phase to larger depths. This hypothesis of molten track formation in iron oxide by the Kr ions is supported by the presence of the nonequilibrium high-temperature wüstite phase, which reflects the extreme conditions in the ion track (high temperature, high pressure) and the rapid resolidification and quenching to the ambient temperature. In the case of the Xe and Au irradiations, the track formation threshold in iron is exceeded, and instead of forming a homogeneous oxide layer, the oxygen from the surface is transported deep into the iron, as seen in the experiment.

If the diffusion takes place only in the hot zone of the excited ion track, the contribution of a single ion (SI) to the experimentally observed diffusion profile (averaged over the spot size A of the analyzing beam) becomes

$$\sigma_{\mathrm{SI}}^2 = (1/A) \int \int 2D(T(r,t))2\pi r dr dt. \tag{3}$$

$D(T(r,t))$ is the temperature-dependent diffusivity of oxygen and $T(r,t)$ describes the temperature profile as a function of the radial distance from the the track center at time t after the ion impact, as obtained from the above-mentioned thermal spike calculations. The effect of N ions randomly distributed over the area A (meaning after irradiation with fluence $\Phi = N/A$) then becomes

$$\sigma^2(\Phi) = N\sigma_{\mathrm{SI}}^2 = 2\pi\Phi \int \int D(T(r,t))2r dr dt. \tag{4}$$

Assuming that efficient diffusion only takes place in the melt with an effective diffusion coefficient D_m, we obtain

$$D' = \sigma^2/\Phi = 2\pi D_m \int r_m^2(t) dt. \tag{5}$$

Again from the thermal spike calculations we get the time-dependent radius $r_m(t)$ of the molten zone shown in Fig. 9. Taking the experimentally determined D' values, we end up with effective diffusion coefficients of $D_m = 0.045$ cm^2/s for 230 MeV Xe and $D_m = 0.126$ cm^2/s for 350 MeV Au.

Similarly high values were reported by Avasthi *et al.*[9] Bester and Lange[30] have published a compilation of thermally activated diffusivities of oxygen and other light atoms in different iron phases. For the melt phase, they report an oxygen diffusion coefficient of some 10^{-4} cm^2/s next to the melting point, which is smaller by a factor of 100–1000 than those we have estimated for SHI-induced diffusion.

There might be various reasons for such discrepancy. Our assumption that the diffusion takes place only above the melting point may be wrong. Considering additional solid-state diffusion in the δ and γ phase of the iron will account only for a factor of 3–5. Moreover, since 180 MeV Kr irradiation does not result in a comparable oxygen diffusion in iron, it can be ruled out that such solid-state diffusion plays a major role, since it should also occur in the hot (but not molten) tracks of the Kr ions. However, in contrast to Kr

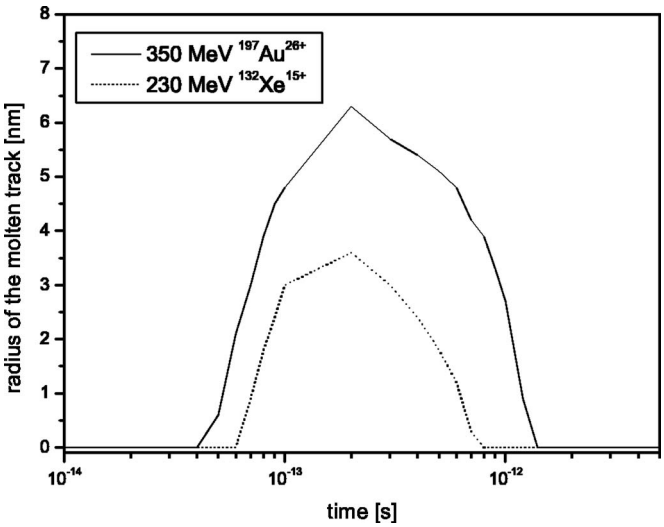

FIG. 9. Radius of the molten track as a function of time after the impact of a 230 MeV Xe ion and a 350 MeV Au ion, as predicted by the thermal spike model.

ions, Xe and Au ions will leave behind lattice defects that might further enhance the diffusivity. We also cannot exclude that the properties of the SHI-induced "melt" differ from the thermally molten iron and exhibit a higher oxygen diffusivity. Although other transport mechanisms such as collective viscous flow rather than atomic diffusion have also been observed in oxides,[31,32] such processes are very unlikely in iron, since they should result in a deformation of the layer, which has not been detected.

V. CONCLUSIONS

We have shown that the oxidation of iron under swift heavy ion bombardment can be mainly ascribed to oxygen transport in the excited ion track, when the stopping power of the ion exceeds the track formation threshold, i.e., when the energy deposition by the ion becomes large enough to overcome the solid binding energies and introduces significant atomic motion. The SHI-induced atomic mixing in oxide layer packages we could recently attribute to transient interdiffusion of the constituent materials in their molten state. Here it is not clear if the incorporation of oxygen into iron under SHI bombardment can be simply regarded as a diffusion process similar to thermally activated indiffusion of oxygen in molten iron, since the estimated SHI-induced diffusion coefficients are larger by a factor of 100–1000 than those reported for thermal diffusion. This point needs further experimental and theoretical work. However, whether oxidation occurs and a homogeneous oxide forms at the surface seems to be governed by the track formation thresholds. Above the track formation threshold of iron, the oxygen is transported deep into the iron and an error-function-like diffusion profile forms. Below the track formation threshold of iron, but still above that of iron oxide, kinetics no longer allow for sufficient oxygen diffusion in iron, and instead a homogeneous oxide phase grows. This oxide phase turns out to be the high-temperature wüstite phase, which reflects the extreme conditions in the molten ion track and the rapid quenching process with cooling rates of the order of $10^{14}-10^{15}$ K/s.

ACKNOWLEDGMENTS

The authors would like to thank H. Paulus, B. Schattat, and S. Klaumünzer for valuable help during the experiments and intensive discussions. The staff of the Ionenstrahllabor of the Hahn-Meitner-Institut Berlin is acknowledged for hospitality and help during the experiments. This work was partly supported by the Deutsche Forschungsgemeinschaft.

*Electronic address: bolse@ifs.physik.uni-stuttgart.de

[1] Nucl. Instrum. Methods Phys. Res. B 244 (2006), edited by D. K. Avasthi and W. Bolse.
[2] Nucl. Instrum. Methods Phys. Res. B 245 (2006), edited by R. Neumann, P. Apel, M. Toulemonde, and C. Trautmann.
[3] R. L. Fleischer, P. B. Price, and R. M. Walker, J. Appl. Phys. **36**, 3645 (1965).
[4] Z. G. Wang, C. Dufour, E. Paumier, and M. Toulemonde, J. Phys.: Condens. Matter **6**, 6733 (1994).
[5] W. Bolse, Radiat. Meas. **36**, 597 (2003).
[6] W. Bolse, B. Schattat, A. Feyh, and T. Renz, Nucl. Instrum. Methods Phys. Res. B **218**, 80 (2004).
[7] B. Schattat and W. Bolse, Nucl. Instrum. Methods Phys. Res. B **225**, 105 (2004).
[8] C. Dais, T. Bolse, B. Schattat, W. Bolse, P. Schubert-Bischoff, and J. K. N. Lindner, Nucl. Instrum. Methods Phys. Res. B **245**, 239 (2006).
[9] D. K. Avasthi, W. Assmann, A. Tripathi, S. K. Srivastava, S. Ghosh, F. Gruner, and M. Toulemonde, Phys. Rev. B **68**, 153106 (2003).
[10] *The Stopping and Range of Ions in Matter*, URL http://www.srim.org.
[11] M. Nastasi and J. W. Mayer, *Ion Solid Interactions* (Cambridge University Press, Cambridge, UK, 1994).
[12] M. Toulemonde, Nucl. Instrum. Methods Phys. Res. B **250**, 263 (2006).
[13] A. Kamarou, E. Wendler, and W. Wesch, J. Appl. Phys. **97**, 123532 (2005).
[14] *Genplot and Rump Homepage*, URL http://www.genplot.com/.
[15] *The iba Datafurnace*, URL http://www.ee.surrey.ac.uk/ibc/ndf/.
[16] K. Nomura, Y. Ujihira, and A. Vértes, J. Radioanal. Nucl. Chem. **202**, 103 (1996).
[17] Y. Maeda, Y. Matsuo, S. Sugihara, N. Momoshima, and Y. Takashima, Corros. Sci. **33**, 1557 (1992).
[18] G. Shirane, D. E. Cox, and S. L. Ruby, Phys. Rev. **125**, 1158 (1961).
[19] A. Muan, Am. J. Sci. **256**, 171 (1958).
[20] R. Beresford, Semicond. Sci. Technol. **18**, 973 (2003).
[21] D. Rafaja and W. Lengauer, Modell. Simul. Mater. Sci. Eng. **6**, 141 (1998).

[22] P. Schaaf (private communication).
[23] A. Dunlop, D. Lesueur, P. Legrand, H. Dammak, and J. Dural, Nucl. Instrum. Methods Phys. Res. B **90**, 330 (1994).
[24] M. Toulemonde, C. Dufour, Z. Wang, and E. Paumier, Nucl. Instrum. Methods Phys. Res. B **112**, 26 (1996).
[25] R. Leguay *et al.*, Nucl. Instrum. Methods Phys. Res. B **106**, 28 (1995).
[26] A. Chettah, Z. G. Wang, M. Kac, H. Kucal, A. Meftah, and M. Toulemonde, Nucl. Instrum. Methods Phys. Res. B **245**, 150 (2006).
[27] C. Rumbolz, W. Bolse, S. Kumar, R. S. Chauhan, D. Kabiraj, and D. K. Avasthi, Nucl. Instrum. Methods Phys. Res. B **245**, 145 (2006).
[28] G. Szenes, Nucl. Instrum. Methods Phys. Res. B **11**, 141 (1996).
[29] M. Martin, W. Mader, and E. Fromm, Thin Solid Films **250**, 61 (1994).
[30] H. Bester and K. W. Lange, Arch. Eisenhuettenwes. **43**, 207 (1972).
[31] S. Klaumünzer and G. Schumacher, Phys. Rev. Lett. **51**, 1987 (1983).
[32] B. Schattat, W. Bolse, S. Klaumünzer, I. Zizak, and R. Scholz, Appl. Phys. Lett. **87**, 173110 (2005).